

6. The Method of Godunov for Non-linear Systems

It was almost 40 years ago when Godunov [130] produced a conservative extension of the first-order upwind scheme of Courant, Isaacson and Rees [89] to non-linear systems of hyperbolic conservation laws. In Chap. 5 we advanced a description of Godunov's method in terms of scalar equations and linear systems with constant coefficients. In this chapter, we describe the scheme for general non-linear hyperbolic systems; in particular, we give a detailed description of the technique as applied to the time-dependent, one dimensional Euler equations. The essential ingredient of Godunov's method is the solution of the Riemann problem, which may be the exact solution or some suitable approximation to it. Here, we present the scheme in terms of the exact solution. In Chaps. 9 to 12 we shall present versions of Godunov's scheme that utilise approximate Riemann solvers; these, if used cautiously, will provide an improvement to the efficiency of the scheme. As seen in Chap. 5 the method is only first-order accurate, which makes it unsuitable for application to practical problems; well-resolved solutions will require the use of very fine meshes, with the associated computing expense. Second and third order extensions of the basic Godunov method will be studied in Chap. 13 for scalar conservation laws; some of these high-order methods are extended to non-linear systems in Chaps. 14 and 16.

Relevant background for studying the Godunov's method is found in all preceding chapters, but detailed review of Chaps. 4 and 5 might be found particularly helpful.

6.1 Bases of Godunov's Method

Consider the general Initial-Boundary Value Problem (IBVP) for non-linear systems of hyperbolic conservation laws

$$\left. \begin{array}{l} \text{PDEs : } \mathbf{U}_t + \mathbf{F}(\mathbf{U})_x = 0, \\ \text{ICs : } \mathbf{U}(x, 0) = \mathbf{U}^{(0)}(x), \\ \text{BCs : } \mathbf{U}(0, t) = \mathbf{U}_l(t), \mathbf{U}(L, t) = \mathbf{U}_r(t). \end{array} \right\} \quad (6.1)$$

Here, $\mathbf{U}(x, t)$ is the vector of conserved variables; $\mathbf{F}(\mathbf{U})$ is the vector of fluxes; $\mathbf{U}^{(0)}(x)$ is the initial data at time $t = 0$; $[0, L]$ is the spatial domain and

boundary conditions are, for the moment, assumed to be represented by the boundary functions $\mathbf{U}_l(t)$ and $\mathbf{U}_r(t)$.

In order to admit discontinuous solutions we must use one of the integral forms of the conservation laws in (6.1). Here we adopt

$$\left. \begin{aligned} \int_{x_1}^{x_2} \mathbf{U}(x, t_2) dx &= \int_{x_1}^{x_2} \mathbf{U}(x, t_1) dx + \int_{t_1}^{t_2} \mathbf{F}(\mathbf{U}(x_1, t)) dt \\ &\quad - \int_{t_1}^{t_2} \mathbf{F}(\mathbf{U}(x_2, t)) dt, \end{aligned} \right\} \quad (6.2)$$

for any control volume $[x_1, x_2] \times [t_1, t_2]$ in the domain of interest; see Sect. 2.4.1 of Chap. 2.

We discretise the spatial domain $[0, L]$ into M computing cells or finite volumes $I_i = [x_{i-\frac{1}{2}}, x_{i+\frac{1}{2}}]$ of regular size $\Delta x = x_{i+\frac{1}{2}} - x_{i-\frac{1}{2}} = L/M$, with $i = 1, \dots, M$. For a given cell I_i the location of the cell centre x_i and the cell boundaries $x_{i-\frac{1}{2}}, x_{i+\frac{1}{2}}$ are given by

$$x_{i-\frac{1}{2}} = (i-1)\Delta x, \quad x_i = i\Delta x, \quad x_{i+\frac{1}{2}} = i\Delta x. \quad (6.3)$$

See Fig. 5.4 of Chap. 5. We denote the temporal domain by $[0, T]$, where T is some output time, not a boundary. The discretisation of the time interval $[0, T]$ is generally done in time steps Δt of variable size; recall that for non-linear systems wave speeds vary in space and time, and thus the choice of Δt is carried out as marching in time proceeds. Given general initial data

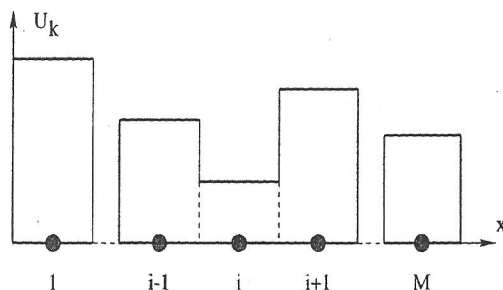


Fig. 6.1. Piece-wise constant distribution of data at time level n , for a single component of the vector \mathbf{U}

$\tilde{\mathbf{U}}(x, t^n)$ for (6.1) at time $t = t^n$ say, in order to evolve the solution to a time $t^{n+1} = t^n + \Delta t$, the Godunov method first assumes a *piece-wise constant* distribution of the data. Formally, this is realised by defining *cell averages*

$$\mathbf{U}_i^n = \frac{1}{\Delta x} \int_{x_{i-\frac{1}{2}}}^{x_{i+\frac{1}{2}}} \tilde{\mathbf{U}}(x, t^n) dx, \quad (6.4)$$

which produces the desired piecewise constant distribution $\mathbf{U}(x, t^n)$, with

$$\mathbf{U}(x, t^n) = \mathbf{U}_i^n, \text{ for } x \text{ in each cell } I_i = [x_{i-\frac{1}{2}}, x_{i+\frac{1}{2}}], \quad (6.5)$$

as illustrated in Fig. 6.1 for a single component \mathbf{U}_k of the vector of conserved variables. Data now consists of a set $\{\mathbf{U}_i^n\}$ of constant states. Naturally these are in terms of conserved variables, but other variables may be derived to proceed with the implementation of numerical methods. In particular, for the Godunov method we use the solution of the Riemann problem in terms of primitive variables, which for the Euler equations are $\mathbf{W} = (\rho, u, p)^T$; ρ is density, u is velocity and p is pressure.

Once the piece-wise constant distribution of data has been established the next step in the Godunov method is to solve the Initial Value Problem (IVP) for the original conservation laws but with the modified initial data (6.5). Effectively, this generates local Riemann problems $RP(\mathbf{U}_i^n, \mathbf{U}_{i+1}^n)$ with data \mathbf{U}_i (left side) and \mathbf{U}_{i+1}^n (right side), centred at the intercell boundary positions $x_{i+\frac{1}{2}}$. As seen for the Euler equations in Chap. 4, the solution of $RP(\mathbf{U}_i^n, \mathbf{U}_{i+1}^n)$ is a similarity solution and depends on the ratio \bar{x}/\bar{t} , see (6.7), and the data states $\mathbf{U}_i^n, \mathbf{U}_{i+1}^n$; the solution is denoted by $\mathbf{U}_{i+\frac{1}{2}}(\bar{x}/\bar{t})$, where (\bar{x}, \bar{t}) are the local coordinates for the local Riemann problem. Fig. 6.2 shows typical wave patterns emerging from intercell boundaries $x_{i-\frac{1}{2}}$ and $x_{i+\frac{1}{2}}$ when solving the two Riemann problems $RP(\mathbf{U}_{i-1}^n, \mathbf{U}_i^n)$ and $RP(\mathbf{U}_i^n, \mathbf{U}_{i+1}^n)$. For

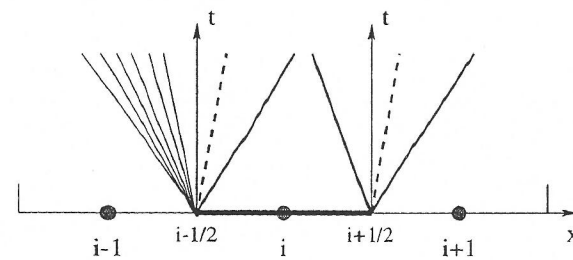


Fig. 6.2. Typical wave patterns emerging from solutions of local Riemann problems at intercell boundaries $i - \frac{1}{2}$ and $i + \frac{1}{2}$

a time step Δt that is sufficiently small, to avoid wave interaction, one can define a global solution $\tilde{\mathbf{U}}(x, t)$ in the strip $0 \leq x \leq L, t^n \leq t \leq t^{n+1}$ in terms of the local solutions as follows

$$\tilde{\mathbf{U}}(x, t) = \mathbf{U}_{i+\frac{1}{2}}(\bar{x}/\bar{t}), \quad x \in [x_i, x_{i+1}], \quad (6.6)$$

where the correspondence between the global (x, t) and local (\bar{x}, \bar{t}) coordinates is given by

$$\left. \begin{aligned} \bar{x} &= x - x_{i+\frac{1}{2}}, & \bar{t} &= t - t^n, \\ x &\in [x_i, x_{i+1}], & t &\in [t^n, t^{n+1}], \\ \bar{x} &\in [-\frac{\Delta x}{2}, \frac{\Delta x}{2}], & \bar{t} &\in [0, \Delta t], \end{aligned} \right\} \quad (6.7)$$

and is illustrated in Fig. 6.3. Having found a solution $\tilde{U}(x, t)$ in terms of solu-

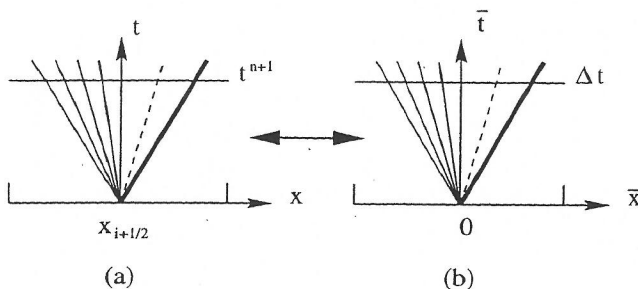


Fig. 6.3. Correspondence between the global (a) and local (b) frames of reference for the solution of the Riemann problem

tions $\mathbf{U}_{i+\frac{1}{2}}(\bar{x}/\bar{t})$ to local Riemann problems, the Godunov method advances the solution to a time $t^{n+1} = t^n + \Delta t$ by defining a new set of average values $\{\mathbf{U}_i^{n+1}\}$, in a way to be described. We shall often use (x, t) to mean the local frame of reference (\bar{x}, \bar{t}) .

6.2 The Godunov Scheme

The first version of Godunov's method defines new average values \mathbf{U}_i^{n+1} at time $t^{n+1} = t^n + \Delta t$ via the integrals

$$\mathbf{U}_i^{n+1} = \frac{1}{\Delta x} \int_{x_{i-\frac{1}{2}}}^{x_{i+\frac{1}{2}}} \tilde{\mathbf{U}}(x, t^{n+1}) dx \quad (6.8)$$

within each cell I_i . This averaging process is illustrated in Fig. 6.4.

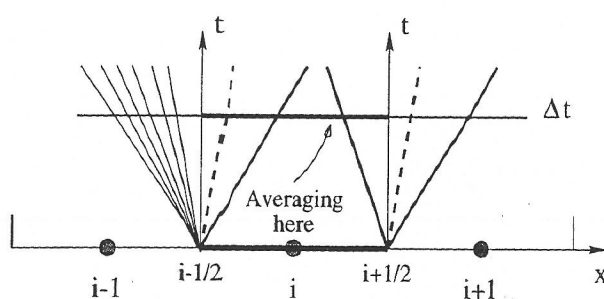


Fig. 6.4. Godunov averaging of local solutions to Riemann problems within cell I_i at a fixed time Δt

Note first that in order to perform the averaging, we need to make the assumption that no wave interaction takes place within cell I_i , in the chosen time Δt . This is satisfied by imposing the following restriction on the size of Δt , namely

$$\Delta t \leq \frac{\frac{1}{2} \Delta x}{S_{\max}^n}, \quad (6.9)$$

where S_{\max}^n denotes the maximum wave velocity present throughout the domain at time t^n . A consequence of this restriction is that only two Riemann problem solutions affect cell I_i , namely the right travelling waves of $\mathbf{U}_{i-\frac{1}{2}}(x/t)$ and the left travelling waves of $\mathbf{U}_{i+\frac{1}{2}}(x/t)$, see Fig. 6.4. Thus \mathbf{U}_i^{n+1} , given by (6.8), can be expressed as

$$\mathbf{U}_i^{n+1} = \frac{1}{\Delta x} \int_0^{\frac{1}{2} \Delta x} \mathbf{U}_{i-\frac{1}{2}}\left(\frac{x}{\Delta t}\right) dx + \frac{1}{\Delta x} \int_{-\frac{1}{2} \Delta x}^0 \mathbf{U}_{i+\frac{1}{2}}\left(\frac{x}{\Delta t}\right) dx, \quad (6.10)$$

after using (6.6) and (6.8). This version of Godunov's method can obviously be implemented as a practical computational scheme. We note however that it has two main drawbacks. First, the CFL-like condition (6.9) is computationally somewhat restrictive on Δt . Second, the evaluation of the integrals in (6.10), although possible, could be involved. Rarefaction waves are bound to add to the complexity of the scheme. The second version of Godunov's method is more attractive and is given by the following statement.

Proposition 6.2.1. *The Godunov method can be written in conservative form*

$$\mathbf{U}_i^{n+1} = \mathbf{U}_i^n + \frac{\Delta t}{\Delta x} [\mathbf{F}_{i-\frac{1}{2}} - \mathbf{F}_{i+\frac{1}{2}}], \quad (6.11)$$

with intercell numerical flux given by

$$\mathbf{F}_{i+\frac{1}{2}} = \mathbf{F}(\mathbf{U}_{i+\frac{1}{2}}(0)), \quad (6.12)$$

if the time step Δt satisfies the condition

$$\Delta t \leq \frac{\Delta x}{S_{\max}^n}. \quad (6.13)$$

Proof. The integrand $\tilde{\mathbf{U}}(x, t)$ in (6.8) is an exact solution of the conservation laws, see equation (6.6). We can therefore apply the integral form (6.2) of the conservation laws to any control volume $[x_1, x_2] \times [t_1, t_2]$. In particular, we can apply it to the case in which $x_1 = x_{i-\frac{1}{2}}$, $x_2 = x_{i+\frac{1}{2}}$, $t_1 = t^n$, $t_2 = t^{n+1}$. From (6.4) we then have

$$\begin{aligned} \int_{x_{i-\frac{1}{2}}}^{x_{i+\frac{1}{2}}} \tilde{\mathbf{U}}(x, t^{n+1}) dx &= \int_{x_{i-\frac{1}{2}}}^{x_{i+\frac{1}{2}}} \tilde{\mathbf{U}}(x, t^n) dx \\ &+ \int_0^{\Delta t} \mathbf{F}[\tilde{\mathbf{U}}(x_{i-\frac{1}{2}}, t)] dt - \int_0^{\Delta t} \mathbf{F}[\tilde{\mathbf{U}}(x_{i+\frac{1}{2}}, t)] dt. \end{aligned} \quad (6.14)$$

In terms of local solutions, as in (6.6), and assuming condition (6.13) we have

$$\left. \begin{aligned} \tilde{U}(x_{i-\frac{1}{2}}, t) &= U_{i-\frac{1}{2}}(0) = \text{constant}, \\ \tilde{U}(x_{i+\frac{1}{2}}, t) &= U_{i+\frac{1}{2}}(0) = \text{constant}, \end{aligned} \right\} \quad (6.15)$$

where $U_{i+\frac{1}{2}}(0)$ is the solution of the Riemann problem $RP(U_i^n, U_{i+1}^n)$ along the ray $x/t = 0$, which is the t-axis in the local frame. Similarly, $U_{i-\frac{1}{2}}(0)$ is the solution of $RP(U_{i-1}^n, U_i^n)$ along the t-axis. Division of (6.14) through by Δx gives

$$\left. \begin{aligned} \frac{1}{\Delta x} \int_{x_{i-\frac{1}{2}}}^{x_{i+\frac{1}{2}}} \tilde{U}(x, t^{n+1}) dx &= \frac{1}{\Delta x} \int_{x_{i-\frac{1}{2}}}^{x_{i+\frac{1}{2}}} \tilde{U}(x, t^n) dx \\ &+ \frac{\Delta t}{\Delta x} [\mathbf{F}(U_{i-\frac{1}{2}}(0)) - \mathbf{F}(U_{i+\frac{1}{2}}(0))], \end{aligned} \right\} \quad (6.16)$$

which by virtue of (6.4) and (6.15) leads to the desired result (6.11)–(6.12), and thus the proposition has been proved.

The following remarks are in order:

- The CFL condition (6.13) for the second version (6.11)–(6.12) of the Godunov method is more generous than (6.9), thus allowing a larger time step. This in turn results in a more efficient time-marching scheme. Here a wave is allowed to travel, at most, a complete cell length Δx in a time Δt .
- Condition (6.13) remains valid even if wave interaction takes place in time Δt within cell I_i , under the assumption that no wave acceleration takes place as a consequence of wave interaction; this is a kind of linearity assumption. Condition (6.13) is necessary in (6.16) when computing the fluxes along the left and right intercell boundaries.
- The second version (6.11)–(6.12) of the Godunov method is the one that is used for practical computations.

6.3 Godunov's Method for the Euler Equations

Here we describe Godunov's method for the specific case of the time-dependent, one-dimensional Euler equations. As data $\{U_i^n\}$ at time level n is assumed, in order to march the solution to time level $n + 1$ via the conservative formula (6.11) we need to compute the intercell fluxes $\mathbf{F}_{i-\frac{1}{2}}$ and $\mathbf{F}_{i+\frac{1}{2}}$.

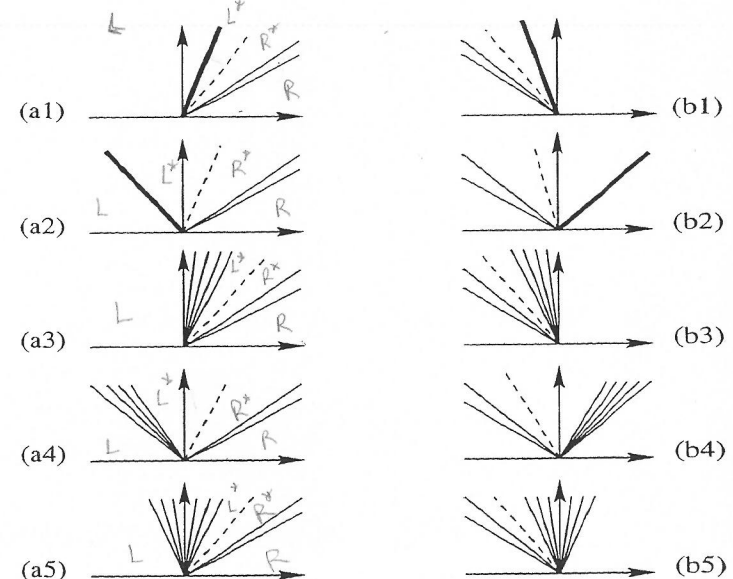


Fig. 6.5. Possible wave patterns in evaluating the Godunov flux for the Euler equations: (a) positive particle speed in the Star Region (b) negative particle speed in the Star Region

6.3.1 Evaluation of the Intercell Fluxes

For a generic cell interface at $x_{i+\frac{1}{2}}$ we compute the Godunov flux $\mathbf{F}_{i+\frac{1}{2}}$ according to (6.12). We therefore require the solution $U_{i+\frac{1}{2}}(x/t)$ of the Riemann problem $RP(U_i^n, U_{i+1}^n)$ evaluated at the point $S = x/t = 0$.

In Chap. 4 we presented the complete exact solution to a general Riemann problem $RP(U_i^n, U_{i+1}^n)$ for the Euler equations. In practice we use the solution in terms of the primitive variables, which we denote by $\mathbf{W}_{i+\frac{1}{2}}(x/t)$. Having found $\mathbf{W}_{i+\frac{1}{2}}(x/t)$ its evaluation at any point $S = x/t$ is carried out by the subroutine SÂMPLE in the FORTRAN 77 program given in Sect. 4.9 of Chap. 4. Sampling requires the identification of ten possible wave patterns; these are illustrated in Fig. 6.5. The flow chart of Fig. 4.14 in Chap. 4 relates to the five cases arising when the sample point S lies to the left of the contact discontinuity. For the Godunov method the sampling is performed for the special value $S = x/t = 0$. Unfortunately, this does not simplify the sampling procedure and all ten possible wave patterns must be taken into account; these are shown in Fig. 6.5. Recall that in our convention a shock is a single thick ray, a contact is a dashed line and a rarefaction wave is obviously a fan. A wave of unknown character is represented by a pair of rays emanating from the origin. There are two situations, each of which has five cases, namely (a) $0 \leq u_*$ (positive particle speed in the Star Region) and

(b) $0 \geq u_*$ (negative particle speed in the *Star Region*). The sampled value $\mathbf{W}_{i+\frac{1}{2}}(0)$ needed for evaluating the Godunov flux is given in Table 6.1 for all ten possible wave patterns; see Fig. 6.5. Consider for example the situation in which u_* is positive. In order to compute correctly the value $\mathbf{W}_{i+\frac{1}{2}}(0)$ along the t -axis (left of contact) we must identify the character of the left wave. This can be a shock, cases (a1) and (a2), or a rarefaction wave, cases (a3), (a4) and (a5). If the left wave is a shock wave we compute the state $\mathbf{W}_{*,L}$ between the left shock and the contact using shock relations, see Sect. 4.5.1 of Chap. 4. Then the speed S_L of the left shock is computed. This then allows us to test whether the shock speed is positive (supersonic flow) or negative (subsonic flow). If $S_L \geq 0$ then

$$\mathbf{W}_{i+\frac{1}{2}}(0) = \mathbf{W}_L.$$

If $S_L \leq 0$ then

$$\mathbf{W}_{i+\frac{1}{2}}(0) = \mathbf{W}_{*,L}.$$

The analysis for the remaining cases (a3) to (a5) is analogous, as is for the set of cases (b1) to (b5). Details are omitted.

Test	Case (a): positive speed u_*	case (b): negative speed u_*
1	\mathbf{W}_L	\mathbf{W}_R
2	$\mathbf{W}_{*,L}$	$\mathbf{W}_{*,R}$
3	\mathbf{W}_L	\mathbf{W}_R
4	$\mathbf{W}_{*,L}$	$\mathbf{W}_{*,R}$
5	$\mathbf{W}_{L\text{fan}}$	$\mathbf{W}_{R\text{fan}}$

Table 6.1. Value of $\mathbf{W}_{i+\frac{1}{2}}(0)$ required for evaluating the Godunov flux, for all ten possible wave patterns in the solution of the Riemann problem

Having identified the desired value $\mathbf{W}_{i+\frac{1}{2}}(0)$ the intercell (6.12) becomes

$$\mathbf{F}_{i+\frac{1}{2}} = \mathbf{F}(\mathbf{W}_{i+\frac{1}{2}}(0)).$$

Exercise 6.3.1. Construct a flow chart for computing the Godunov flux for the time-dependent, one-dimensional Euler equations.

Solution 6.3.1. (Left to the reader).

Exercise 6.3.2. Draw all possible wave patterns required for evaluating the Godunov flux for the isentropic equations of Gas Dynamics; see Sect. 2.4.4 of Chap. 4. Construct a flow chart for computing the Godunov flux.

Solution 6.3.2. (Left to the reader).

6.3.2 Time Step Size

So far we know how to compute the intercell flux (6.12) to be used in the conservative formula (6.11). The spatial discretisation length Δx is chosen on desired accuracy or available computing resources. What remains to be determined in (6.11) is the size of the time step Δt . This is based on the condition (6.13). The time step is then given by

$$\Delta t = \frac{C_{\text{cfl}} \Delta x}{S_{\max}^n}. \quad (6.17)$$

Here C_{cfl} is a Courant or CFL coefficient satisfying

$$0 < C_{\text{cfl}} \leq 1. \quad (6.18)$$

The closer the coefficient C_{cfl} is to 1, the more efficient the time marching scheme is. S_{\max}^n is the largest wave speed present throughout the domain at time level n . This means that no wave present in the solution of all Riemann problems travels more than a distance Δx in time Δt . As discussed in Chap. 5 in the context of simple problems, there are various ways of estimating S_{\max}^n . For the time-dependent, one dimensional Euler equations a reliable choice is

$$S_{\max}^n = \max_i \{ |S_{i+\frac{1}{2}}^L|, |S_{i+\frac{1}{2}}^R| \}, \quad (6.19)$$

for $i = 0, \dots, M$, where $S_{i+\frac{1}{2}}^L, S_{i+\frac{1}{2}}^R$ are the wave speeds of the left and right non-linear waves present in the solution of the Riemann problem $RP(U_i^n, U_{i+1}^n)$. Recall that this Riemann problem generates three waves; the fastest are the non-linear waves, which can be shocks or rarefactions. For rarefaction waves one selects the speed of the head. For shock waves one selects the shock speed, naturally. Note that in sampling the wave speeds one must include the boundaries, as these might generate large wave speeds. Using (6.19) to find S_{\max}^n and thus Δt according to (6.17), is a simple and very reliable procedure. As the local solutions of Riemann problems are available for flux evaluation, it is just a question of using this information to find Δt as well. For multi-dimensional problems however, this scheme for estimating the maximum wave speed is unsuitable; see Sect. 16.3.2 of Chap. 16.

A popular alternative for estimating S_{\max}^n , which extends to multi-dimensional problems, is

$$S_{\max}^n = \max_i \{ |u_i^n| + a_i^n \}. \quad (6.20)$$

Only data values for the particle velocity u_i^n and sound speed a_i^n are used here. It is not difficult to see however that (6.20) can lead to an underestimate of S_{\max}^n . For instance, assume shock-tube data in which the flow is stationary at time $t = 0$. Then $u_i^n = 0$ and the sound speed is the only contribution to S_{\max}^n . Underestimating S_{\max}^n results in a choice of Δt that is too large and instabilities may be developed from the beginning of the computations.

A possible way of remedying this, is by choosing the CFL coefficient C_{CFL} in (6.17) cautiously. If S_{\max}^n is known reliably then the choice $C_{\text{CFL}} = 1$ is probably adequate, although this implies that waves pass through each other without acceleration, which is a kind of linearity assumption. A practical choice is $C_{\text{CFL}} = 0.9$. If there are uncertainties in the estimate of S_{\max}^n , such as when (6.20) is used, a more conservative choice for C_{CFL} is advised. In spite of the alluded disadvantages of choice (6.20), it provides a practical approach when computing solutions to multi-dimensional problems. See Chap. 16.

6.3.3 Boundary Conditions

For a domain $[0, L]$ discretised into M computing cells of length Δx we need boundary conditions at the boundaries $x = 0$ and $x = L$ as illustrated in Fig. 6.6. Numerically, such boundary conditions are expected to provide numerical fluxes $\mathbf{F}_{\frac{1}{2}}$ and $\mathbf{F}_{M+\frac{1}{2}}$. These are required in order to apply the conservative formula (6.11) to update the extreme cells I_1 and I_M to the next time level $n + 1$. The boundary conditions may result in direct prescription of $\mathbf{F}_{\frac{1}{2}}$ and $\mathbf{F}_{M+\frac{1}{2}}$. Alternatively, we may have *fictitious data values* in the fictitious cells I_0 and I_{M+1} , adjacent to I_1 and I_M respectively; see Fig. 6.6. In this way, boundary Riemann problems $RP(\mathbf{U}_0^n, \mathbf{U}_1^n)$ and $RP(\mathbf{U}_M^n, \mathbf{U}_{M+1}^n)$ are solved and the corresponding Godunov fluxes $\mathbf{F}_{\frac{1}{2}}$ and $\mathbf{F}_{M+\frac{1}{2}}$ are computed, as done for the interior cells. The imposition of boundary conditions is, fundamentally,

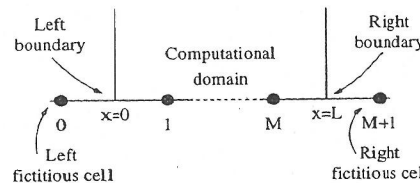


Fig. 6.6. Boundary conditions. Fictitious cells outside the computational domain are created

a physical problem. Great care is required in their numerical implementation. For the Godunov method this task tends to be facilitated by the fact that local Riemann problem solutions are used. Here we consider only two types of boundaries: *reflective* and *transparent* or *transmissive*.

Reflective Boundaries. Consider the boundary at $x = L$ and suppose it physically consists of a fixed, reflective impermeable wall. Then the physical situation is correctly modelled by creating a fictitious state \mathbf{W}_{M+1}^n on the right hand side of the boundary and defining the boundary Riemann problem $RP(\mathbf{W}_M^n, \mathbf{W}_{M+1}^n)$. The fictitious state \mathbf{W}_{M+1}^n is defined from the known state \mathbf{W}_M^n inside the computational domain, namely

$$\rho_{M+1}^n = \rho_M^n, \quad u_{M+1}^n = -u_M^n, \quad p_{M+1}^n = p_M^n. \quad (6.21)$$

By symmetry

The exact solution of this boundary Riemann problem consists of either (i) two shock waves if $u_M^n > 0$ or (ii) two rarefaction waves if $u_M^n \leq 0$. In both cases $u_* = 0$ along the boundary; this is the desired condition at the solid, fixed impermeable boundary. Consequently, the only non-zero contribution to the flux vector at the boundary is in the momentum component and is due to the pressure p_* corresponding to $u_* = 0$. In both cases the solution can be obtained in closed form, no iteration is required. As a matter of fact, a closed-form solution exists for the more general case in which the fluid under consideration obeys the covolume equation of state and the impermeable wall moves with a prescribed speed u_{wall} [323]. The boundary conditions are

$$\rho_{M+1}^n = \rho_M^n, \quad u_{M+1}^n = -u_M^n + 2u_{\text{wall}}, \quad p_{M+1}^n = p_M^n. \quad (6.22)$$

The exact solution of the Riemann problem $RP(\mathbf{W}_M^n, \mathbf{W}_{M+1}^n)$ containing a moving boundary is symmetric about the path of the moving wall and consists of either (a) two shocks or (b) two rarefactions, with the contact wave coinciding with the moving wall, as desired. See Fig. 6.7.

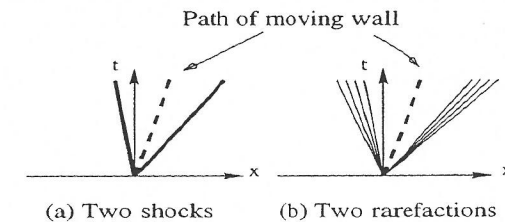


Fig. 6.7. Boundary Riemann problem for moving wall. Contact surface coincides with moving solid boundary: (a) solution consists of two shocks and the contact (b) solution consists of two rarefactions and the contact

From the analysis of the exact function for pressure, see Sect. 4.3 of Chap 4, it is seen that if $\Delta u = -2(u_M - u_{\text{wall}}) = 0$, that is $u_M = u_{\text{wall}}$, then the solution p_* for pressure at the boundary is $p_* = p_M = p_{M+1}$. For $\Delta u > 0$ we have $p_* < p_M = p_{M+1}$, that is, the solution consists of two rarefaction waves, see Fig. 6.7b. For $\Delta u < 0$ we have $p_* > p_M = p_{M+1}$ and the solution consists of two shocks, see Fig. 6.7a. For the case of two rarefaction waves, $u_M \leq u_{\text{wall}}$, direct utilisation of the data into the pressure function $f(p) = 0$, see Sect. 4.3 of Chap 4, gives

$$p_* = p_M \left[1 + \frac{1}{2}(\gamma - 1) \left(\frac{C_M}{a_M} \right) \right]^{\frac{2\gamma}{\gamma-1}}. \quad (6.23)$$

For the case of two shocks, $u_M > u_{\text{wall}}$, we have

$$p_* = p_M + \frac{C_M}{2A_M} \left\{ C_M + [C_M^2 + 4A_M(B_M + p_M)]^{\frac{1}{2}} \right\}, \quad (6.24)$$

where

$$A_M = \frac{2}{(\gamma + 1)\rho_M}, \quad B_M = \frac{(\gamma - 1)}{(\gamma + 1)}p_M, \quad C_M = u_M - u_{\text{wall}}. \quad (6.25)$$

As anticipated, the solution for the velocity u_* in both cases is found to be

$$u_* = u_{\text{wall}}. \quad (6.26)$$

These closed-form solutions for the pressure and velocity at the boundary (fixed or moving) can also be utilised in conjunction with approximate Riemann solvers, particularly if these are thought to be inaccurate for boundary data Riemann problems. A useful discussion on solid-body boundary conditions for the Euler equations in multi-dimensional domains is given by Rizzi [252]. A recommended paper on boundary conditions for hyperbolic problems is that of Thompson [321].

Transmissive Boundaries. Transmissive, or transparent boundaries arise from the need to define finite, or sufficiently small, computational domains. The corresponding boundary conditions are a numerical attempt to produce boundaries that allow the passage of waves without any effect on them. For one-dimensional problems the objective is reasonably well attained. For multi-dimensional problems this is a substantial area of current research, usually referred to as *open-end* boundary conditions, *transparent* boundary conditions, *far-field* boundary conditions, *radiation* boundary conditions or *non-reflecting* boundary conditions. For a transmissive right boundary we suggest the boundary conditions

$$\rho_{M+1}^n = \rho_M^n, \quad u_{M+1}^n = u_M^n, \quad p_{M+1}^n = p_M^n. \quad (6.27)$$

This data produces a trivial Riemann problem. No wave of finite strength is produced at the boundary that may affect the flow inside the domain. Useful publications dealing with transparent boundary conditions are those of Giles [120], Bayliss and Turkel [20], Roe [261] and Karni [173].

For an assumed mesh of size Δx , we have defined all details for the practical implementation of the Godunov method, see (6.11)–(6.13). These are

- intercell fluxes
- the maximum wave speed S_{\max}^n to compute the time step size Δt , and
- boundary conditions.

Remark 6.3.1. The wave speeds generated at the boundaries, after applying boundary conditions, must be taken into account when selecting the time step Δt .

Exercise 6.3.3. Write a flow chart to implement the Godunov method to solve the one-dimensional, time dependent Euler equations in a tube of constant cross sectional area. Assume the left wall is impermeable and fixed and the right wall is transparent.

Solution 6.3.3. (Left to the reader).

6.4 Numerical Results and Discussion

Here we assess the performance of Godunov's first-order upwind method for the Euler equations on test problems with exact solution. For comparison we also show numerical results obtained by the Lax-Friedrichs and Richtmyer methods, discussed in Chap. 5. In all chosen tests, data consists of two constant states $\mathbf{W}_L = (\rho_L, u_L, p_L)^T$ and $\mathbf{W}_R = (\rho_R, u_R, p_R)^T$, separated by a discontinuity at a position $x = x_0$. The states \mathbf{W}_L and \mathbf{W}_R are given in Table 6.2. The ratio of specific heats is chosen to be $\gamma = 1.4$. The exact and numerical solutions are found in the spatial domain $0 \leq x \leq 1$. The numerical solution is computed with $M = 100$ cells and the Courant number coefficient is $C_{\text{cfl}} = 0.9$; boundary conditions are transmissive and S_{\max}^n is found using the simplified formula (6.20).

Remark 6.4.1. Given that formula (6.20) is not reliable, see discussion in Sect. 6.3.2, in all computations presented here we take, for the the first 5 time steps, a Courant number coefficient C_{cfl} reduced by a factor of 0.2. This allows for waves to begin to form, after which formula (6.20) becomes more reliable.

Test	ρ_L	u_L	p_L	ρ_R	u_R	p_R
1	1.0	0.75	1.0	0.125	0.0	0.1
2	1.0	-2.0	0.4	1.0	2.0	0.4
3	1.0	0.0	1000.0	1.0	0.0	0.01
4	5.99924	19.5975	460.894	5.99242	-6.19633	46.0950

Table 6.2. Data for four test problems with exact solution

Test 1 is a *modified version* of the popular Sod's test [291]; the solution consists of a right shock wave, a right travelling contact wave and a left *sonic* rarefaction wave; this test is very useful in assessing the *entropy satisfaction* property of numerical methods. Test 2 has solution consisting of two symmetric rarefaction waves and a trivial contact wave of zero speed; the *Star Region* between the non-linear waves is close to vacuum, which makes this problem a suitable test for assessing the performance of numerical methods for low-density flows; this is the so called *123 problem* introduced in chapter Chap. 4. Test 3 is designed to assess the robustness and accuracy of numerical methods; its solution consists of a strong shock wave, a contact surface and a left rarefaction wave. Test 4 is also designed to test robustness of numerical methods; the solution consists of three strong discontinuities travelling to the right. See Sect. 4.3.3 of Chap. 4 for more details on the exact solution of these test problems. For each test we select a convenient position x_0 of the initial discontinuity and the output time. These are stated in the legend of each figure displaying computational results.

Figs. 6.8 to 6.11 show comparisons between exact solutions (line) and numerical solutions (symbol) at a given output time obtained by the Godunov method, for all four test problems. The quantities shown are density ρ , particle speed u , pressure p and specific internal energy e . For comparison, we also solved these test problems using the Lax–Friedrichs method, see Figs. 6.12 to 6.15, and the the Richtmyer method. This latter method failed to provide a solution to Tests 2 to 4. For Test 1 the solution is shown in Fig. 6.16.

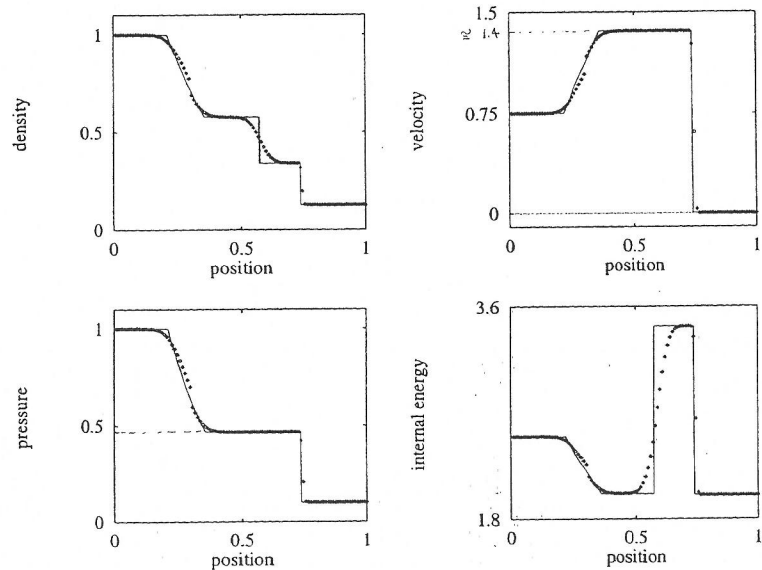


Fig. 6.8. Godunov's method applied to Test 1, with $x_0 = 0.3$. Numerical (symbol) and exact (line) solutions are compared at the output time 0.2 units

6.4.1 Numerical Results for Godunov's Method

The results for Test 1, shown in Fig. 6.8, are typical of the Godunov's first-order accurate method described in this chapter.

The numerical approximation of the shock wave, of zero-width transition in the exact solution, has a transition region of width approximately $4\Delta x$; that is, the shock has been *smeared* over 4 computing cells. This spreading of shock waves may seem unsatisfactory, but it is quite typical of numerical solutions; in fact most first-order methods will spread a shock wave even more. A satisfactory feature of the numerical shock wave of Fig. 6.8 is that it is monotone, there are no spurious oscillations in the vicinity of the shock, at least

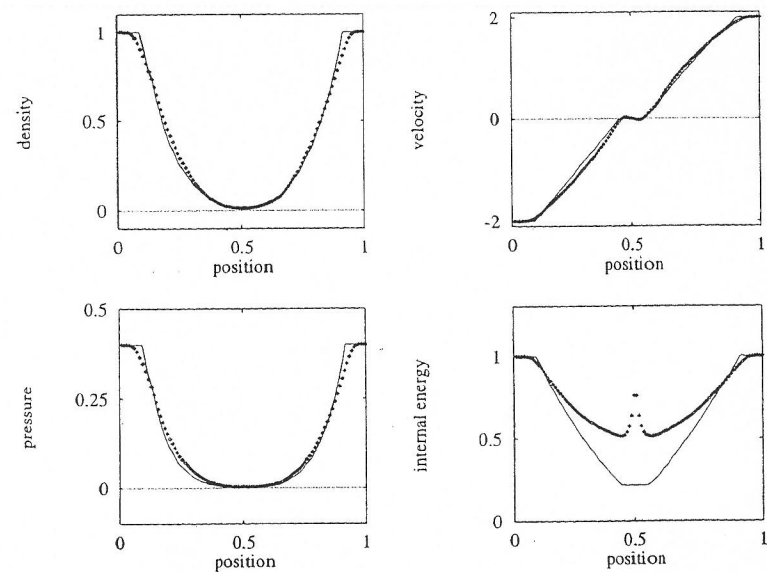


Fig. 6.9. Godunov's method applied to Test 2, with $x_0 = 0.5$. Numerical (symbol) and exact (line) solutions are compared at the output time 0.15 units

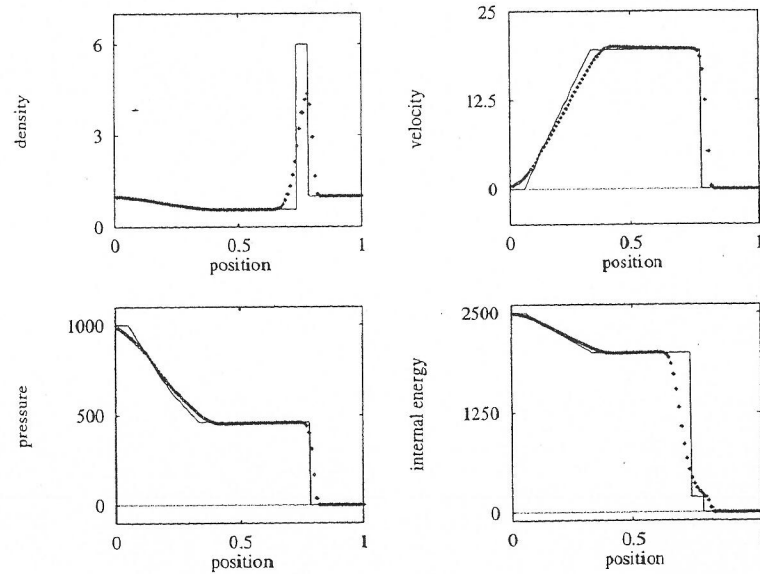


Fig. 6.10. Godunov's method applied to Test 3, with $x_0 = 0.5$. Numerical (symbol) and exact (line) solutions are compared at the output time 0.012 units

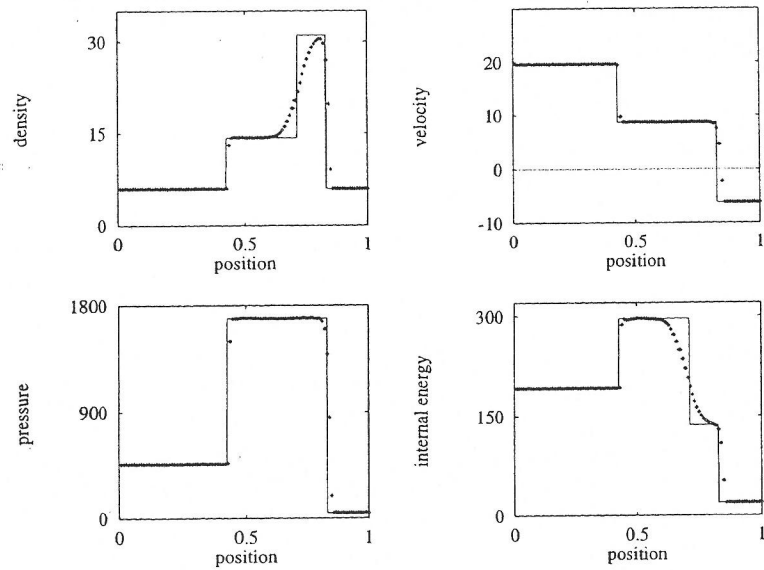


Fig. 6.11. Godunov's method applied to Test 4, with $x_0 = 0.4$. Numerical (symbol) and exact (line) solutions are compared at the output time 0.035 units

for this example. Monotonicity of shock waves computed by the Godunov method depends on the speed of the shock and it holds in most cases except when the shock speed is very close to zero. The contact discontinuity, seen in the density and internal energy plots, is smeared over 20 cells; generally contact waves are much more difficult to resolve accurately than shock waves. This is due to the linear character of contacts; characteristics on either side of the wave run parallel to the wave. In shock waves characteristics on either side of the wave run into the shock, a compression mechanism that helps the numerical resolution of shock waves. As for the shock case, the solution for the contact is perfectly monotone.

Another positive feature of the numerical approximation of the discontinuities is that their speed of propagation is correct and thus their average positions are correct. This is a consequence of the conservative character of Godunov's method. The rarefaction wave is a smooth flow feature and is reasonably well approximated by the method except near the head and the tail, where a discontinuity in derivative exists. Another visible error in the rarefaction is the small discontinuous jump within the rarefaction. This is sometimes referred to as the *entropy glitch* and arises only in the presence of sonic rarefaction waves, as in the present case. Godunov's method is theoretically entropy satisfying [148] and we therefore expect the size of the jump in the entropy glitch to tend to zero as the mesh size Δx tends to zero.

The performance of Godunov's method on Test 2, see Fig. 6.9, is generally quite satisfactory as regards the physical variables p , u and ρ but not so much for the specific internal energy, which is computed from ρ and p as $e = p/((\gamma - 1)\rho)$. In this low density example both pressure and density are close to zero and thus small errors will be exaggerated by their ratio. In any case, it is generally accepted that plots of the internal energy e can be quite revealing of the quality of the numerical solution. On the other hand pressure is probably the easiest quantity to get right. The main point of Test 2 is to make the reader aware that this class of low density flows can easily cause numerical methods to fail; even the robust Godunov method fails if used in conjunction with certain approximate Riemann solvers [106]. The Richtmyer method fails to give a solution to this problem.

Test 3 is a very severe problem and is designed to test the robustness of the Godunov method, the results of which are shown in Fig. 6.10. The emerging right travelling shock wave has pressure ratio $p_*/p_R = 46000$ and a corresponding shock Mach number of 198. For flows involving such strong shock waves as this, one would seriously question the validity of the ideal gas equations of state. However, from the point of view of assessing the robustness of numerical schemes, this is not a problem. As for Test 1, the resolution of discontinuities is worst for the contact wave; as a consequence of this, post shock values are not attained, as is clearly seen in the density plot. The velocity plot shows a kind of overshoot near the tail of the rarefaction. The Richtmyer scheme failed for this test.

As seen in Fig. 6.11 the solution of Test 4 consists of three discontinuities: two shock waves and a contact. They all travel to the right; the left shock has a small positive speed. The complete wave system has resulted from the interaction of two strong shock waves propagating in opposite directions. The right shock is the fastest wave and is smeared over 5 cells, as seen in the pressure plot; the left, slowly moving shock is sharply resolved (two cells) but is not monotone; there are some *low frequency* spurious oscillations in its vicinity, as seen in the internal energy plot. The contact discontinuity is heavily smeared. Slowly moving shocks are sharply resolved by Godunov's method; in fact, both shocks and contacts of zero speed are perfectly resolved, if non-defective Riemann solvers are used, see Chap. 10. The phenomenon of spurious oscillations in slowly moving shocks has been studied by Roberts [254] and is so far, to the author's knowledge, an unresolved difficulty. Billett and Toro [37] investigated some possible cures of the problem for the Euler equations. See also the recent paper by Arora and Roe [13].

6.4.2 Numerical Results from Other Methods

First we apply the Lax-Friedrichs method, see Sect. 5.3.4 of Chap. 5, to Tests 1 to 4. The numerical results are shown in Figs. 6.12 to 6.15. The results for Test 1 are shown in Fig. 6.12 and are to be compared with those of Godunov's method, Fig. 6.8. The Lax-Friedrichs scheme has the peculiar property of